JOURNAL OF PROPULSION AND POWER
Vol. 18, No. 4, July–August 2002

Inlet/Compressor System Response to Short-Duration Acoustic Disturbances

Anthony B. Opalski* and Miklos Sajben†
University of Cincinnati, Cincinnati, Ohio 45221-0070

Recent studies have shown that computations of unsteady high-speed inlet flows produce results that strongly depend on the compressor-face boundary condition. Traditionally applied boundary conditions have no experimental verification, which leads to uncertainty and significant risks in development programs. Experimental information is offered that can serve as a basis for constructing realistic boundary conditions. Short-duration transients were investigated in a constant-area circular inlet attached to an operating high-speed, single-stage, axial flow compressor. The transients were initiated by the generation of short-duration acoustic pulses within the inlet, using an exploding wire method. Pulse duration was typically 2 ms, with a peak amplitude of 3% of the mean inlet static pressure measured at the compressor face. Fast-response wall-mounted pressure transducers were used to detect the incident, reflected, and transmitted pulses. Data were obtained for axial compressor-face Mach numbers from 0.15 to 0.45. Frequency-domain analysis was used to extract dimensionless transfer functions that may be viewed as frequency-resolved reflection and transmission coefficients. The information is appropriate for the characterization of the compressor face for computational purposes. None of the customary boundary conditions predict the data obtained in this study, highlighting the need to revise conventional methods of imposing outflow boundary conditions.

Nomenclature

a	=	speed of sound
C	=	capacitance
d	=	duct diameter
E	=	initial energy level
f	=	frequency, Hz
$H[f]$	=	frequency-response function, $Z[f]/Y[f]$
M	=	axial Mach number
N	=	rotational speed, rpm
P	=	static pressure
P'	=	perturbation in static pressure, $P - P_0$
R	=	resistance
T	=	period
t	=	time
u	=	velocity
V	=	initial voltage level
x	=	axial location, zero at leading edge of nose cone, positive in downstream direction
$Y[f]$	=	Fourier transform of input time history, $y(t)$; incident acoustic disturbance
$Z[f]$	=	Fourier transform of output time history, $z(t)$; reflected or transmitted disturbance
Δt	=	time shift
δ^*	=	displacement thickness
τ	=	time delay
$\phi[f]$	=	phase angle, rad

Subscripts

CF	=	compressor face value
e	=	edge (or core flow) value
i	=	index value
RRP	=	reference reflection plane value
0	=	undisturbed value at compressor face

Presented as Paper 2001-3885 at the AIAA/ASME/SAE/ASEE 37th Joint Propulsion Conference, Salt Lake City, UT, 8–11 July 2001; received 14 August 2001; revision received 7 February 2002; accepted for publication 14 February 2002.

*Graduate Research Assistant, Department of Aerospace Engineering and Engineering Mechanics; opalskab@email.uc.edu. Student Member AIAA.

†Professor Emeritus, Department of Aerospace Engineering and Engineering Mechanics; mmsajben@fuse.net. Fellow AIAA.

Introduction

HIGHLY sophisticated and extensively tested computational fluid dynamic (CFD) codes are available to simulate the steady/unsteady operation of inlets and compressors in airbreathing propulsion devices. In contrast, the methods used to combine these codes for predicting the unsteady behavior of a coupled inlet/compressor system are in a significantly less advanced state, and engineering practice typically relies on single-component CFD codes. The work presented here addresses the problem of representing the compressor as a boundary condition when using an inlet code for simulating a rapid inlet/compressor system transient.

Unsteady inlet flows in gas-turbine engines are of concern to aircraft designers for several reasons. Transients occur in normal operation, induced by changes in aircraft speed or incidence angle, and aircraft passage through gusts, shear layers, temperature stratifications, or microscale turbulence.[1,2] Disturbances within the inlet of supersonic fighter aircraft can be generated by rapid maneuvers, as well as ingestion of combustibles from gun/missile firings. Control system changes, including throttling and ramp angle adjustments, introduce perturbations, some of which can be very rapid.

In all such processes, the inlet and engine dynamically influence each other, and the correct prediction of the resultant system behavior requires that this mutual interaction be considered. The difficulties of performing such a time-dependent numerical analysis of a coupled inlet/compressor system are enormous and so far have been performed only as research projects. Engine designers working in a development environment must utilize individual component codes in which the adjacent components are represented via boundary conditions. Figure 1 illustrates a typical computational domain utilized for unsteady inlet flow computations, with the engine dynamics represented via the compressor face boundary condition (CFBC).

In the mid-1990s the increasing sophistication of CFD methods permitted systematic queries into this issue and verified that the choice of the CFBC does indeed have a major effect on the solution.[3,4] From a programmatic point of view, answers that depend strongly on questionable inputs represent significant risks that may mandate increased safety margins, which usually degrade the overall performance of the system.

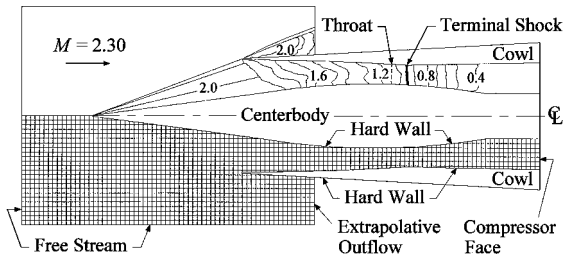

Fig. 1 Conditions imposed at the boundaries of the computational domain of an axisymmetric mixed-compression supersonic inlet: upper half shows Mach contours; lower half shows computational domain.

Traditional Boundary Conditions

Until recently, the practice has been to use boundary conditions that have been traditionally applied to steady-state operation on the basis of simple intuitive arguments and mathematical convenience. Most of these conditions assume that a selected flow variable is temporally constant at the outflow boundary. The variables that have been chosen include static pressure, axial velocity, axial Mach number, corrected mass flow, etc. Unfortunately, no experimental verification supports any of these conditions, and the quality of representation afforded by them is open to doubt.[5]

If the timescale of the transient is sufficiently long to permit the assumption of quasi steadiness, then it is appropriate to use engine performance maps to define time-dependent boundary conditions.[6] Unfortunately, some of the changes mentioned in the preceding section occur far too fast for a quasi-steady description to apply. There is a need to determine what conditions exist at the compressor face during a truly unsteady transient.

The lack of experimental data relevant to this problem is attributable in part to the general difficulty of the subject. Apparently the inlet/engine interface, falling squarely between the inlet and compressor design groups, has never received the focused attention of either. It was not until 1994 that a clearly defined experimental plan of attack, centered on an impulse method of measuring acoustic impedance, was conceived and formulated.[7] New experimental methods were invented and developed[8] to implement the envisioned experiment, utilizing a coupled inlet/compressor system. The effort was successful, and a series of papers[9–13] followed that described the results obtained with a 10-stage compressor, at inlet axial Mach numbers up to 0.18. The experimentally detected responses were quite different from those predicted by customary boundary conditions. The findings clearly indicated that current practices concerning outflow boundary conditions are in need of revision.

The present work is an extension of the research described in Refs. 7–13. The approach taken in the current work and the manner in which it differs from the earlier studies are described in the next section.

Approach

Small disturbances associated with the motion of a compressible fluid may be decomposed into three components[14]: entropy, vorticity, and acoustic modes. If the disturbance scales are small and the mean flow is uniform, then each of these modes is governed by an independent equation.

This modal decomposition is also convenient experimentally because it is relatively easy to create nearly pure entropy, vortical, or acoustic disturbances. The compressor responses may then be determined by a separate experiment for each disturbance type. The present research effort was aimed at the experimental characterization of engine response to acoustic and entropy disturbances. The present paper reports on the acoustic results; entropy disturbances are the subject of another publication.[15]

The technique selected for the exploration of compressor response was the impulse method.[16] This method requires that a short-duration disturbance of the desired type be generated in the inlet and be allowed to propagate (or convect) to the compressor face. When it arrives at the compressor, some response is generated that may contain all three disturbance types. However, the entropy and vorticity disturbances are always convected into the engine, and only the acoustic response has an upstream-moving part. It is this response that actually affects the inlet flow, and it is the focus of our interest.

The duration of the reflection process can be made sufficiently short such that it is completed before secondary disturbances or reverberations from other parts of the inlet can reach the compressor face. The impulse method, thus, makes it possible to isolate temporally the basic reflection from other, nonrelevant processes. In contrast to the impulse method, a periodic excitation would create an overall oscillatory flow pattern whose properties would depend on the entire inlet flow, including all geometrical details and the upstream boundary conditions. It would be very difficult, if not impossible, to extract compressor-face characterizations from such data.

Unlike the low-speed, multistage compressor work described in Refs. 9–13, the present work employed a single-stage engine and the range of inlet flow conditions was extended to axial Mach numbers up to 0.45, which is more representative of modern engine design practices. Additionally, the measurement of transmission coefficients was made possible through the use of an outlet duct extending downstream of the engine assembly.

Concept of Experiment

The realization of the project's objectives demanded a facility and a pulse-generation method that satisfied the following requirements: 1) a very nearly planar, downstream-moving acoustic pulse of 1–2 ms duration must be generated; 2) the acoustic pulse magnitude must be sufficiently large to be clearly detectable over the intense engine noise, especially at the blade passing frequency; 3) the system must generate an entropy pulse of readily detectable magnitude; 4) an outlet duct to allow the measurement of transmission coefficients must be included; and 5) the duct lengths and the relative positions of the engine and the pulse generator device must be such that the pulses of interest can be clearly isolated.

The pulse-generation requirements were met by an exploding wire technique, in which a single wire located in the inlet (perpendicular to the flow and fully spanning the diameter) is vaporized by a short-duration current pulse. Activation of the pulse generator creates a pair of acoustic compression waves, one traveling upstream toward the bellmouth and one traveling downstream toward the compressor. Only the downstream-moving wave is needed: The upstream-moving wave is merely a nuisance, but, fortunately, is a manageable one.

The rapid heating of the air during the discharge also creates an entropy disturbance simultaneously. The entropy pulse convects at the flow speed, which is much lower than that of the acoustic pulses, and the entropy pulse arrives at the compressor much later than the acoustic pulse. This temporal separation permits the study of both response types while using the same pulse-generation method.

The inlet used for this experiment is a long, constant area duct, as shown in Fig. 2a. This duct obviously does not simulate a real inlet, but this is not necessary because interest is focused on the compressor-face location. The constant area keeps the flow well behaved and leads to pulses that propagate without appreciably changing their shapes.

When a pulse reaches either end of the system, reflections are generated that propagate through the system in the opposite direction. The processes are illustrated in the x–t diagram (Fig. 2b). The diagram shows how the difference between the entropy and acoustic wave speeds permits the isolation of the respective processes from each other. The duct lengths and compressor/pulse generator locations that offer the cleanest separation depend on the Mach number. The dimensions finally chosen (and shown in Fig. 2) represent a compromise that allows operation at all selected Mach numbers (0.15–0.45) for tests involving acoustic disturbances.

The downstream-moving acoustic pulses are labeled as DP-1, DP-2, etc., whereas the upstream-moving acoustic pulses are UP-1, UP-2, etc., with numbering beginning with their order of appearance. Note that after passage through the compressor, the incident DP-1 pulse becomes the transmitted DP-2 pulse. The DP-1 $\rightarrow$ UP-2 reflection and DP-1 $\rightarrow$ DP-2 transmission are of principal interest.

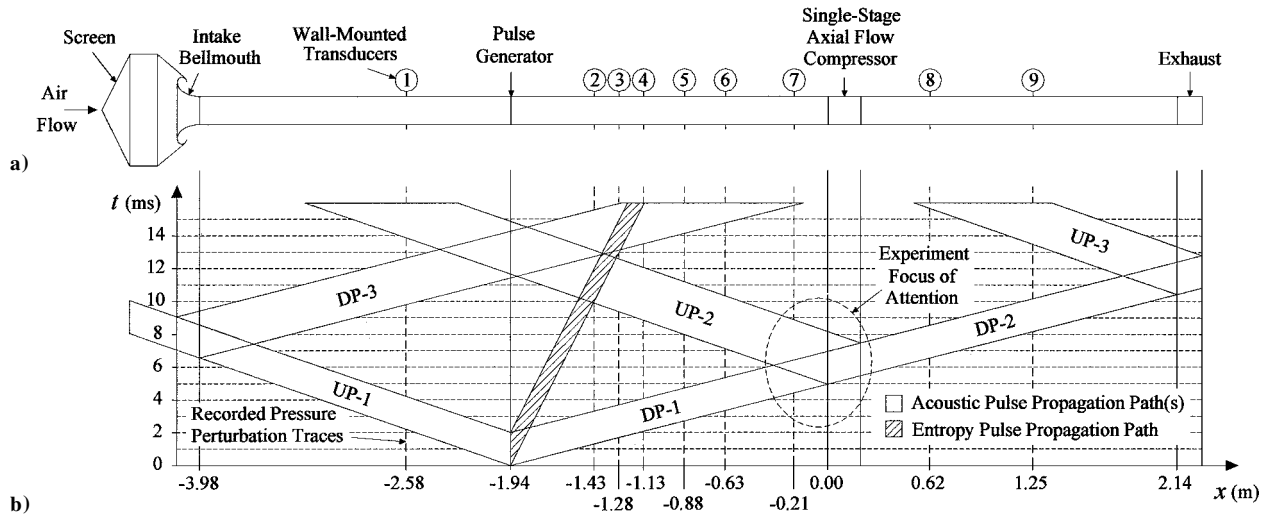

Fig. 2 Distance-time (x–t) diagram illustrating propagation of pulses in constant-area circular inlet assembly, $M_{CF} = 0.15$.

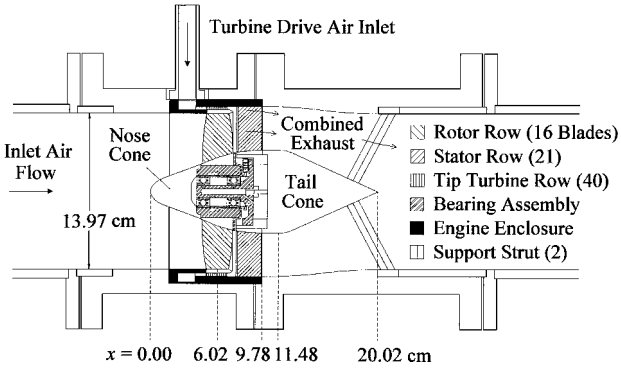

Fig. 3 Details of single-stage axial flow compressor assembly.

Table 1 TDI-457 engine geometry information (measured)

		Rotor		Stator		Turbine	
Parameter	Location	Inlet	Outlet	Inlet	Outlet	Inlet	Outlet
Blade radii, cm	Hub	2.45	3.49	3.62	3.81	7.32	7.32
	Mean	4.72	5.24	5.62	5.72	7.45	7.45
	Tip	6.99	6.99	7.62	7.62	7.58	7.58
Blade angles, deg	Hub	37	0	−37	12	−45	45
	Mean	44	28	−31	12	−45	45
	Tip	52	41	−22	12	−45	45
Blade chords, cm	Hub	2.63	——	2.13	——	1.78	——
	Mean	2.68	——	2.13	——	1.78	——
	Tip	2.72	——	2.13	——	1.78	——
Axial chords, cm	Hub	2.63	——	2.10	——	1.78	——
	Mean	2.55	——	2.10	——	1.78	——
	Tip	2.00	——	2.10	——	1.78	——

Description of Experimental Facilities

The work was carried out in the Fluid Mechanics and Propulsion Laboratory of the Department of Aerospace Engineering and Engineering Mechanics, located on the campus of the University of Cincinnati (UC). The major elements of the test facility constructed for the purposes of this program include the compressor (fan), the inlet, the pulse generator, and data acquisition systems.

Compressor

The compressor (Fig. 3) is a propulsion simulator engine manufactured by Tech Development, Inc., of Dayton, Ohio (TDI Model 457). It is a single-stage, tip-turbine driven axial flow compressor with a constant rotor tip diameter of 13.97 cm (5.50 in.). A nose cone attached to the rotor provides the transition from circular to annular cross section. A stationary blade row and a stator tail cone complete the assembly. The engine housing is designed to mate with the inlet facility. An annular plenum chamber with 33 integral guide vane nozzles is used to distribute drive air to an array of 40 turbine blades attached to a shroud surrounding the rotor blade tips. High-pressure, filtered air, heated to eliminate blade icing, is supplied from an external source to the plenum chamber. The turbine drive air passes through the stator blade row and mixes with the core fan airflow. The combined exhaust stream discharges to the atmosphere after passing through the outlet duct segment.

The engine speed and, hence, inlet Mach number are controlled by varying the stagnation pressure to the turbine inlet. Speed could be set and held within ±200 rpm using a dedicated proportional–integral–derivative controller, corresponding to Mach number control with a tolerance of ±0.002.

The nominal design point of the installed engine is at a total pressure ratio of 1.25 at a corrected speed of 35,400 rpm, with a fan inlet airflow of 2.34 kg/s (5.17 lbm/s). This corresponds to a mass-flow-averaged compressor-face axial Mach number of 0.45. The turbine drive airflow at the design point is 0.50 kg/s (1.10 lbm/s) at an inlet stagnation pressure and temperature of 2.41 MPa (350 psia) and 345 K (160°F), respectively. The total combined outflow is 2.84 kg/s.

The rotor has 16 blades with inlet and outlet hub-to-tip radius ratios of 0.35 and 0.50, respectively. The blades have a moderate twist, and the solidity and stagger angle at the mean diameter are 1.45 and 18 deg, respectively. The stator has 21 blades with a tip diameter of 15.24 cm (6.00 in.), with inlet and outlet hub-to-tip radius ratios of 0.475 and 0.50. The stator diameter is larger than that of the rotor to accommodate the turbine exhaust. A transitional contour of the outer wall directly downstream of the stator reduces the outlet duct diameter to that of the inlet duct and also accommodates smooth mixing of the turbine discharge air with the fan core airflow. Details of the engine design are summarized in Table 1.

The UC Fluid Mechanics and Propulsion Laboratory is equipped with an air supply system capable of delivering pressure, temperature, and humidity controlled turbine drive air. The system has sufficient capacity to allow continuous engine operation.

Inlet Duct

Figure 2a shows the compressor mated with the 13.97-cm-diam constant-area inlet/outlet assembly. The lengths of the inlet and exhaust duct segments are 3.84 m (151.0 in.) and 1.94 m (76.3 in.), respectively. The air enters the inlet through a filtered bellmouth screen installed to prevent the entry of environmentally generated

flow nonuniformities into the system. Two wall-mounted boundary-layer trip rings force transition to turbulent flow over the complete inlet Mach number range. The trips are identical: Both have 1 mm height and 1 mm width. They are located 10 and 40 cm downstream of the end of the bellmouth, respectively.

Pulse Generator

Located near the midpoint of the inlet is a pulse generator whose operation is based on the explosion of a single, very thin, high resistivity wire oriented normal to the flow direction (spanning the duct diameter from top to bottom). The explosion is initiated by a rapid current discharge through the wire from a high-voltage (up to 5 kV) dc energy storage capacitor (9.9 μF). When the current carrying capacity of the wire is exceeded, joule heating quickly raises the wire temperature until vaporization occurs.

The principal components of the pulse generating system include a simple resistance–capacitance (RC) charging circuit connecting the capacitor to the dc power supply and an isolated high-voltage discharge relay connecting the capacitor to the test wire. The overall design was based on the need to generate a temperature disturbance (entropy pulse) with a peak temperature increase equal to 10% of the absolute temperature of the gas. The energy input required for this purpose was quite sufficient for the simultaneous generation of acoustic pulses with the desired magnitude (3% of the mean static pressure). The strength of the pulses depended on the initial energy stored in the capacitor, $E = 1/2CV^2$, that is, on the initial capacitor voltage level. Energy inputs up to 125 J are possible, but the tests presented here all used 79.2 J (obtained at $V = 4$ kV).

The wire mounting assembly comprises two conducting bars inlayed horizontally into an insulating plate, each centered directly above and below the inlet duct. Each bar has a screw arrangement to connect 15.24-cm- (6.00-in.-) long wires across the duct span and external connections to the RC discharge circuit are provided. A spacer plate is affixed to the top of the mounting plate to seal the assembly to the inlet duct. The upstream inlet section can be moved to allow the removal of the entire unit for wire replacement.

The wire filaments used in the experiment were 25.4-μm- (0.001-in.-) diam carbon fiber coated with a 25.4-μm-thick layer of silicon carbide (50%Si/50%C). Manufactured by Textron Systems under the trade name SCS-9, the filament is a nonmetallic ceramic–matrix composite (mainly used for composite material reinforcement). Testing has shown this wire type to outperform other heating element types, including Ni/Cr alloys. The advantages include higher resistivity (11.1 kΩ/m), lower thermal inertia (necessary for rapid heating), a higher melting temperature (2400°C), and a more uniform composition (repeatability of pulses).

Additionally, the carbon fiber provides stiffness and a high tensile strength (3.45 GPa) necessary to withstand the dynamic loads imposed by the inlet airflow. The carbon cores of the wires typically remained in place following a test. Although the explosion process introduces fine-grain solid mass into the flow (due to the incomplete vaporization of all of the silicon carbide coating), the quantity is negligible in comparison to the air mass flow.

The experiments reported in this paper used the downstream moving incident pulse (DP-1) to study the processes occurring at the compressor face. This pulse is a compression wave with an approximately 2.0-ms duration and a typical magnitude near 3% of the mean static pressure measured at the compressor face. The pulse-generation process also results in higher frequency oscillations, occurring at a reduced amplitude level and decaying quite rapidly. Some of these are thought to be associated with transverse modes present at higher frequencies (above 3 kHz). As will be discussed later, these higher frequency contributions could be removed through filtering during data processing and did not degrade the experiment.

Instrumentation and Data Acquisition

Steady-State Data

The inlet assembly was instrumented with 50 static pressure taps to determine the characteristics of the mean flow. The compressor was instrumented with pressure, temperature, and speed sensors to monitor overall performance. Barometric pressure and ambient temperature were recorded throughout each test. All steady-state parameters of the inlet and the engine were recorded at a 2-kHz data rate using a 16-bit data acquisition board (National Instruments AT-MIO-16X).

Dynamic Data

A total of four fast-response Entran pressure transducers (Model EPI-080, 34.5-kPa range, 120-kHz natural frequency, $\pm 1\%$ full-scale accuracy) were flush mounted on the walls of the inlet duct, both upstream and downstream of the compressor. The transducers were located at the nine axial stations indicated on Fig. 2. The azimuthal location of all transducers was 45 deg clockwise, referenced from 0 deg located at top dead center (looking downstream). A 12-bit, 1-MHz throughput data acquisition board (National Instruments AT-MIO-16E-1) was used to acquire the high-speed pressure data. All dynamic data were digitized at 125 kHz per channel.

All signals were amplified and fed from the facility through an instrumentation trench to an adjacent control room. National Instruments LabVIEW software (version 4.0), running on a Pentium-based personal computer, was used to acquire all data, control the experiment, and perform most of the data analysis.

Test Procedure

Because the pulse-generation technique is a one-shot event, installation of the wire was performed before each run. Following engine speed-up to operating conditions, a continuity/resistance check was performed to verify the wire was still intact. The charging circuit was then activated, and the capacitor was charged to the specified voltage level. Approximately 2 s before discharging the capacitor, steady flow parameters in the inlet and engine were recorded to determine the initial steady-state conditions. The high-speed data system was also activated for a short time, to provide an accurate reading of the undisturbed wall static pressures at each transducer location.

The discharge relay was then activated and data acquisition was simultaneously triggered off the relay energization signal, which was strong enough to induce a spike in all transducer readings. The presence of the spikes ensured that the wire explosion (occurring typically 1–2 ms after triggering) could be easily identified in all recorded signals. Following data collection for approximately 80 ms (until the dynamic processes had subsided), the steady flow parameters of the inlet and engine were again recorded, along with data from the high-speed transducers. The steady-state conditions and the undisturbed static pressures for the high-response transducers presented here represent the average of readings taken before and after the transient. A data acquisition portion of a run generally required only 90 s for completion.

Results

Time Mean Flow

Measurements of velocity profiles were made in the inlet duct to characterize the uniformity of the inlet flow, using a translating five-arm total pressure rake. Results at three axial locations (corresponding to positions near the inlet bellmouth, pulse generator, and compressor face) for $M_{CF} = 0.30$ are shown in Fig. 4. The calculated displacement thicknesses corresponding to these locations are $\delta^* = 0.7$, 3.3, and 5.8 mm, respectively. Blockage values ($=2\delta^*/d$) calculated from these data at the pulse generator and compressor face yield blockages of 4.8 and 8.3%, respectively. The relatively thick boundary layer near the entrance is a consequence of the first boundary-layer transition ring located at $x = -373.55$ cm (11 cm upstream of the first traverse location). The blockage is relatively large at the compressor face, due to the large length/diameter ratio of the inlet duct. However, no appreciable diffusion of the wave profile was observed, nor did the profile nonuniformity have a significant effect on the acoustic wave speed.

Similar profiles (not shown) were seen at $M_{CF} = 0.15$ and 0.45, which is expected because the effect of velocity on the thickness of

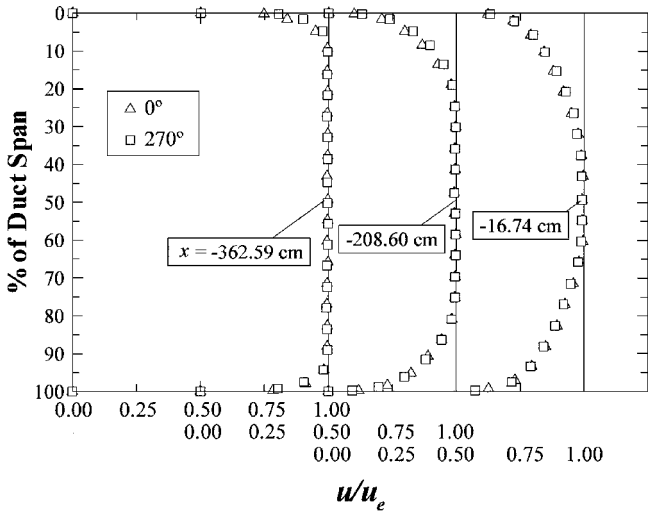

Fig. 4 Velocity profiles at three axial positions in the inlet, $M_{CF} = 0.30$.

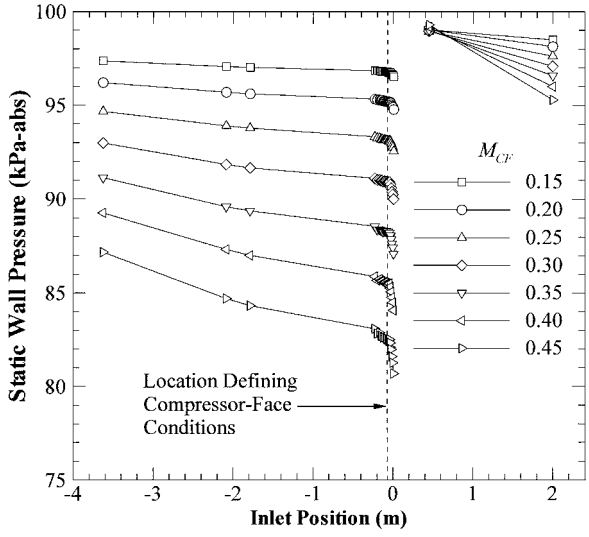

Fig. 5 Axial static pressure distributions in the inlet assembly.

the turbulent boundary layer is relatively weak (thickness is approximately proportional to the $-\frac{1}{5}$ power of the edge velocity).

Figure 5 shows the resulting static pressure distributions in the facility over the complete range of inlet flow conditions. The profiles upstream of the compressor clearly show the influence of the engine nose cone on the static pressure profile near the compressor face. The location of the nominal compressor face ($x_{CF} = -6.21$ cm) was chosen to avoid this nose cone effect. The profiles downstream of the compressor were generated from data collected at only two axial stations, so the resulting shapes (straight lines) shown are only approximations of the true axial static pressure distributions.

The compressor-face Mach numbers presented here were determined in the following manner. To account for the slight pressure drop across the bellmouth screen, a single pitot probe (immersed by 2.54 cm, well into the core flow) recorded total pressure at $x = -362.59$ cm. In combination with eight static wall pressure readings measured at the same axial location (equally spaced around the duct perimeter and manifolded together for a single average reading), the entrance core flow conditions where found. By the use of the Fanno flow relations with atmospheric temperature as total temperature, and an average static pressure reading at the compressor face (again from eight equally spaced perimeter taps manifolded together at $x = -6.21$ cm), the total pressure drop and, hence, a compressor face Mach number, could be found.

Time-Dependent Data

After a careful study of the power spectra of all signals, a cutoff frequency of 2.75 kHz was chosen for low-pass filtering of the high-speed data. This process effectively removed nearly all compressor and flow noise, while retaining the processes associated with the pulses. The data processing method is described hereafter for the case of $M_{CF} = 0.15$.

The overall structure of the wave patterns observed is illustrated in Fig. 6, in terms of typical time histories of wall static pressures at nine locations in the inlet. Each trace is an average measurement resulting from five runs with transducers located at each position. Figure 6 is similar in structure to the x–t diagram shown in Fig. 2, but the vertical distances among the individual traces are not accurately proportional to the respective distances. The time traces of Fig. 6 correspond to data taken along vertical lines in Fig. 2, at the axial stations 1–9. Figure 2 shows that pulses moving in opposite directions may be superimposed, but that the occurrence of such events is limited to small regions of the x–t diagram by the appropriate choice of duct lengths and transducer locations. Figure 6g illustrates a superposition of DP-1 and UP-2 pulses, showing that the signal is then complex and the structures of the contributing pulses are not readily identifiable. As expected, the duct ends behave like constant pressure terminations and generate reflections of opposite signs.

Incident Pulse (DP-1)

Figure 7 shows five filtered DP-1 signals taken from five different runs, with the same transducer (station 3, see Fig. 2 for transducer locations) and for the same engine conditions. The close overlap demonstrates the high degree of repeatability of the pulse-generation process. The pulse-generation process was repeatable for a given Mach number, but the peak pressure slightly decreased with increasing Mach number. This was of no concern, because the wave/engine interaction process was demonstrated to be closely linear, and the response characteristics do not appreciably depend on the pulse magnitude.

Figure 8 shows filtered DP-1 pulses from six different stations located between the pulse generator and compressor (stations 2–7). The time record of the pressure perturbation at station 2 is left unchanged, but the others have been shifted backward in time and the UP-2 pulse overlaps edited (removed) from the traces. The removal starts at the instant the leading edge of the UP-2 pulse arrives at the given transducer location, as noted by the vertical lines in Fig. 8. The time shift for the trace obtained at the ith location was calculated as follows:

$$(\Delta t)_i = \frac{x_i - x_2}{a + u} = \frac{x_i - x_2}{a_{CF}(1 + M_{CF})} \tag{1}$$

that is, the magnitude of the shift is equal to the time of propagation from station 2 to station i. The wave speed was calculated from time-mean measurements of M and a at the compressor face, independently of the high-speed data. As illustrated in Fig. 5, the static pressure and, hence, the static temperature change throughout the duct, and the speed of sound is not truly constant. However, analyses utilizing a variable speed of sound results in a maximum time shift deviation within $\pm 1.5\%$ of the value used here, and so no appreciable error is introduced by assuming that the wave speed is constant along the upstream duct section between the pulse generator and compressor.

Figure 8 allows two important conclusions. First, the pulse shape remains accurately constant and is not attenuated or diffused during propagation from station 2 to station 7. Second, the speed of propagation can be computed accurately from the mean flow properties.

Figure 9 shows filtered DP-1 pulses from two runs and two axial stations (2 and 7). For each run, the transducers were placed at four equally spaced azimuthal positions to check on pulse axisymmetry near the pulse generator and compressor face. The dual peak in the data at station 7 is created by the superposition of pulses DP-1 and UP-2 (cf. Fig. 2). Figure 9 allows the conclusion that both the incident and the reflected pulses are axisymmetric to a high degree, at least near the compressor face.

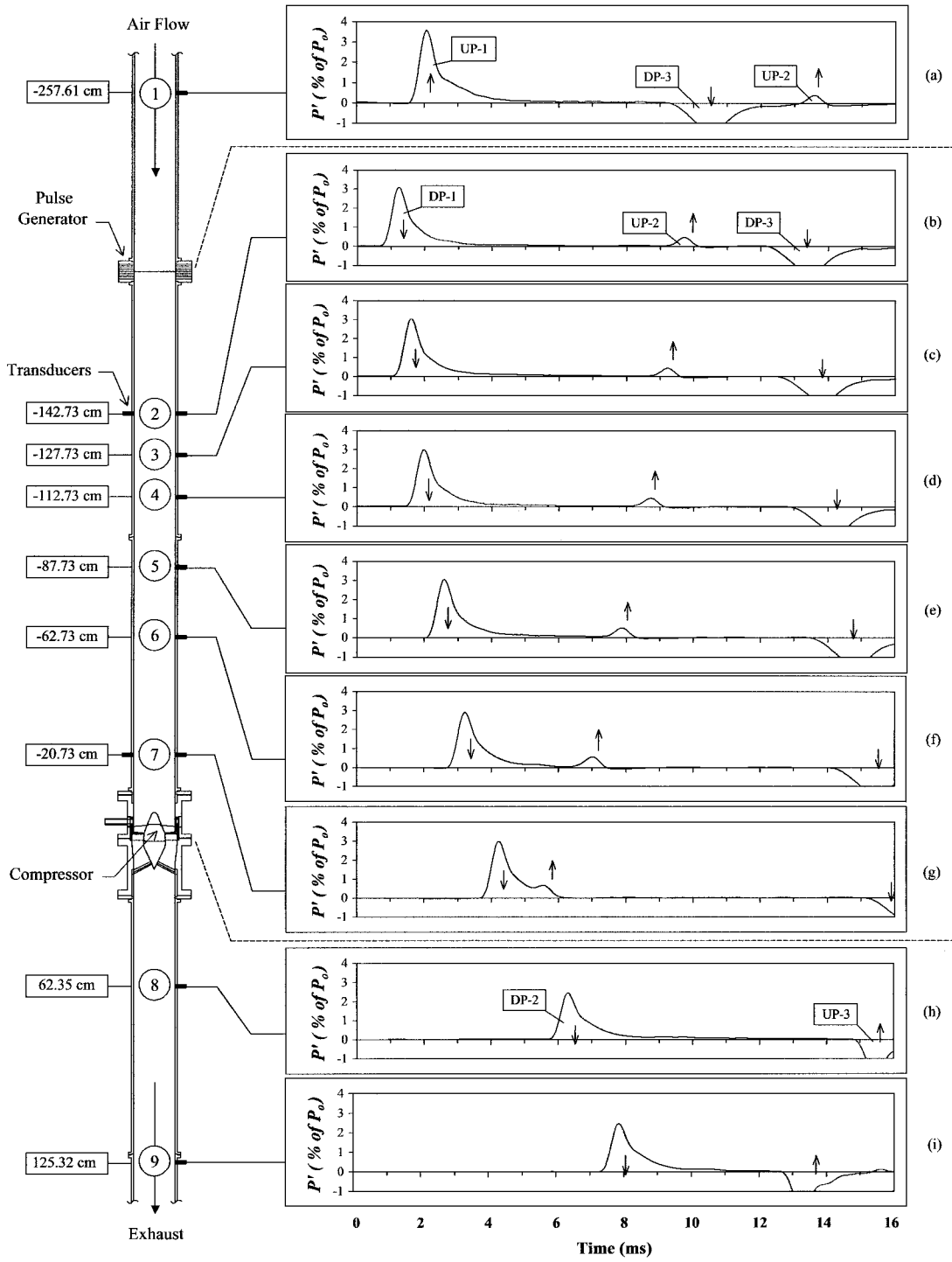

Fig. 6 Temporal evolution of static pressure in the inlet assembly at $M_{CF} = 0.15$; vertical arrows indicate direction of propagation of the disturbances.

Reflected Pulse (UP-2)

The superposition of five UP-2 pulses is shown in Fig. 10. By the use of the trace at station 2 again as a reference, traces from stations 3–6 were shifted to later times by the following intervals:

$$(\Delta t)_i = \frac{x_2 - x_i}{a - u} = \frac{x_2 - x_i}{a_{CF}(1 - M_{CF})} \tag{2}$$

The DP-3 pulses are of no interest in this context and were edited from the signals by replacing them with zeros. The average of the traces in Figs. 8 and 10 were used to characterize the DP-1 → UP-2 reflection. To compare the response to the incident pulse directly in the time domain, the average UP-2 pulse was shifted backward in time by

$$\Delta t = \frac{x_2 - x_{\mathrm{RRP}}}{a_{CF}(1 - M_{CF})} - \frac{x_{\mathrm{RRP}} - x_2}{a_{CF}(1 + M_{CF})} \tag{3}$$

where the reference reflection plane (RRP) is chosen as the tip of the engine nose cone (that is, $x = 0$). This time shift corresponds to the downstream propagation of DP-1 from station 2 to the RRP and the upstream propagation of UP-2 from the RRP back to station 2. This procedure results in Fig. 11, which also includes data at Mach numbers of 0.30 and 0.45, processed in the same manner. Both the incident and reflected pulses were normalized by the peak value of

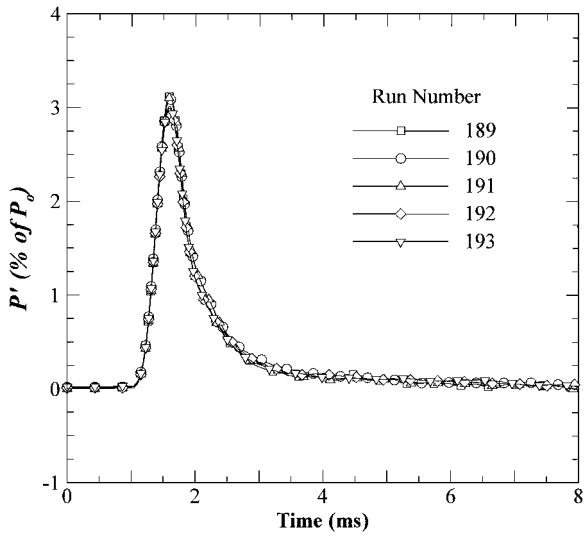

Fig. 7 Comparison of DP-1 profiles at station 3 from five runs, $M_{CF} = 0.15$.

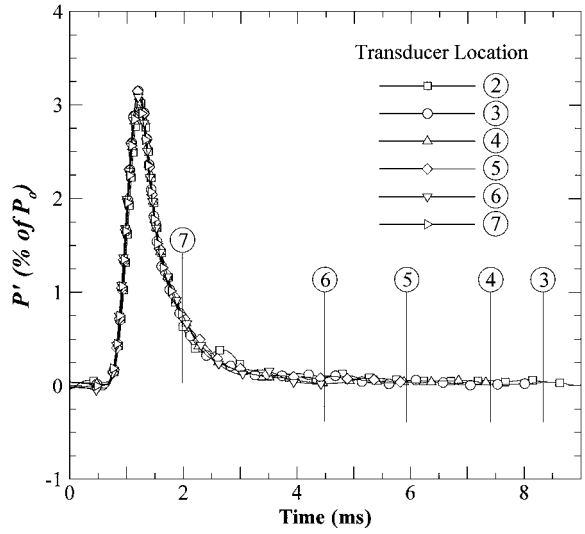

Fig. 8 Comparison of DP-1 profiles at six locations; vertical lines indicate the instant when the leading edge of UP-2 arrives at each transducer location, $M_{CF} = 0.15$.

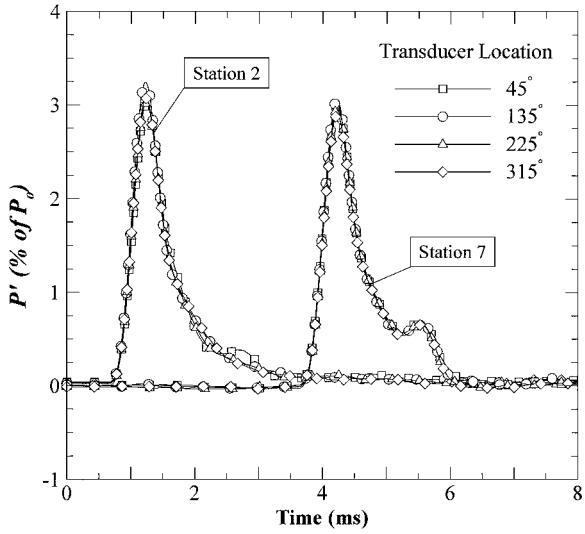

Fig. 9 Axisymmetry of DP-1 pulses at two axial stations, $M_{CF} = 0.15$.

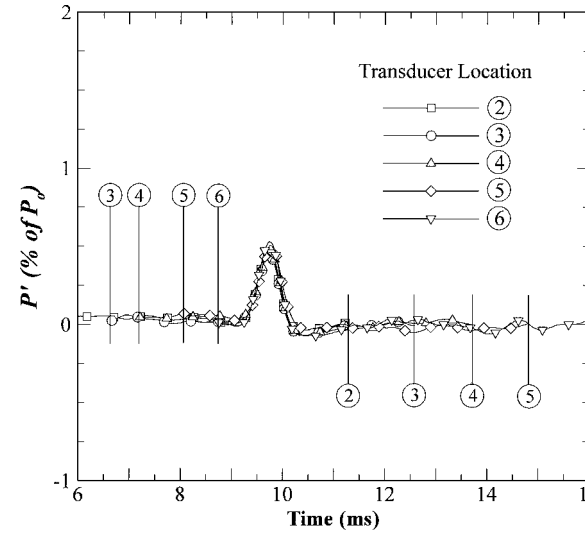

Fig. 10 Comparison of UP-2 at five locations; vertical lines indicate the instant when the leading edge of DP-3 arrives at each transducer location, $M_{CF} = 0.15$.

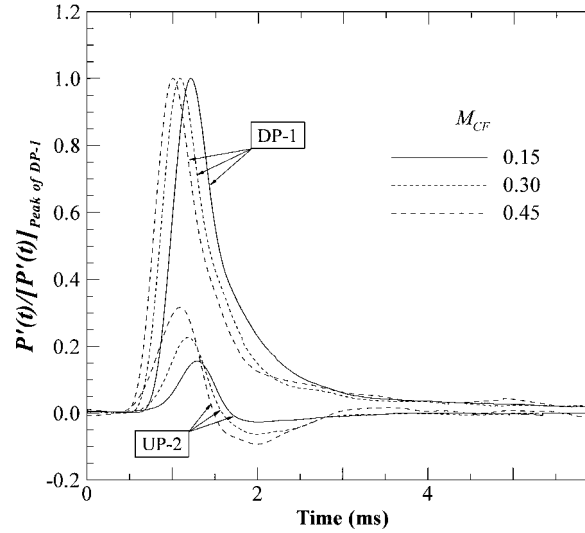

Fig. 11 Averages of DP-1 → UP-2 reflections.

the respective DP-1 pulses. The shifting of the incident/reflection pulse pairs to earlier times with increasing Mach number is the result of the faster wave propagation speeds at higher Mach numbers.

Figure 11 shows that the beginning of the (shifted) reflection and the incident pulses coincide in time. From this we can conclude that 1) the reflected pulse propagates at the wave speed appropriate for an upstream moving planar wave and 2) the RRP was an appropriate choice in defining the region responsible for initiating the reflection.

A notable feature of the reflected pulse is that it is composed of a positive and a subsequent negative part, the result being reminiscent of a single period of a strongly damped sine wave. Because the incident pulse has a simple, unipolar shape with no change of sign, the more complex structure of the reflection requires some explanation.

Reference 17 treats the reflection of planar acoustic waves interacting with a local area change in otherwise constant-area duct flows. It is shown that an area reduction produces reflections of the same sign, and an area increase leads to reflections of opposite sign, with an attenuation dependent on the upstream Mach number. The streamwise distribution of the cross-sectional areas in the engine investigated here may be characterized as an 11.48-cm-long area reduction (the nose cone plus the rotor and stator), followed by an 8.52-cm-long area increase (the tail cone). The reflections of Fig. 11 do indeed display an initially positive disturbance, followed

by a negative one after a time delay. The delay closely equals the time needed for a wave to propagate from the RRP to the beginning of the divergent section and then back to the RRP, as expected on the basis of the proposed explanation.

The duration of the reflection is approximately the same as that of the incident pulse for all Mach numbers and contains contributions from the disturbance interacting with both area changes, as well as the rotor and stator rows. The contributions of the rotor and stator blades to the reflection are both expected to be positive.[17] The shape of the UP-2 pulse suggests that the overall reflection is strongly affected by the area changes.

Transmitted Pulse (DP-2)

In a reflection process the incident and reflected pulses both propagate in the upstream mean flow. In a transmission process, the incident pulse propagates in the upstream mean flow, but the transmitted pulse moves in the downstream flow. This difference in mean flow properties has a significant influence on the characteristics of the transmitted pulse.[17] The differences between the upstream and downstream mean flows also raised a number of questions concerning the appropriate normalization of the transmitted pulse. Consideration of these issues led to the conclusion that the most meaningful normalization is obtained by referencing all disturbances to the peak value of the incident wave (DP-1).

A second issue was the determination of the temporal relationship between the incident and transmitted pulses. The wave moving from station 7 to station 8 passes through, and is modified by, the engine. The wave motion is no longer a simple propagation in a constant-area duct, and a simple expression analogous to Eq. (3) cannot be used to account for the propagation times. The issue was resolved by shifting the trace of the transmitted wave back in time by the amount required to line up its leading edge with that of the incident wave. This time delay was obtained from the unsteady data, without any recourse to the mean flow properties.

Figure 12 shows the average DP-2 traces recorded from five runs at two stations in the exhaust duct, located downstream of the compressor. The bands surrounding the average line correspond to the maximum/minimum data point scatter, again showing the excellent repeatability achieved by the pulse generation process and the consistent operating characteristics of the engine.

The trace at station 9 was aligned with that of station 8, an average taken, and the resulting average DP-2 pulse was then shifted back in time to align it with the average DP-1 pulse at station 2. The result is displayed in Fig. 13 for $M_{CF} = 0.15$, 0.30, and 0.45. To eliminate the overlapping of the various Mach number cases, each pair of traces was shifted forward in time by 1 ms, in addition to the earlier manipulations.

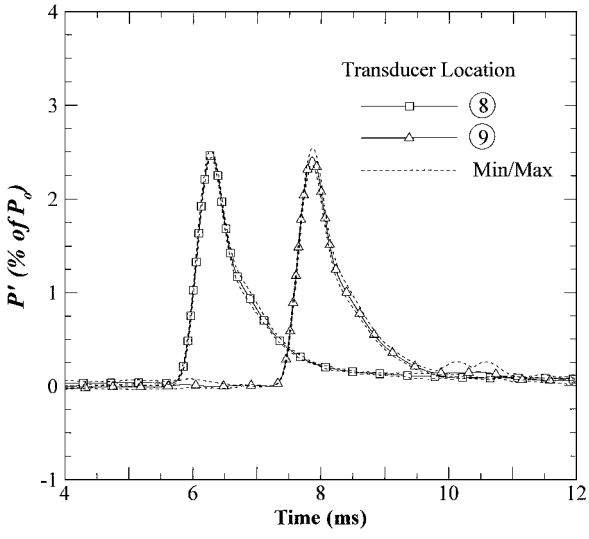

Fig. 12 Comparison of average transmitted (DP-2) profiles from five runs at two locations; bands represent minimum/maximum data point range, $M_{CF} = 0.15$.

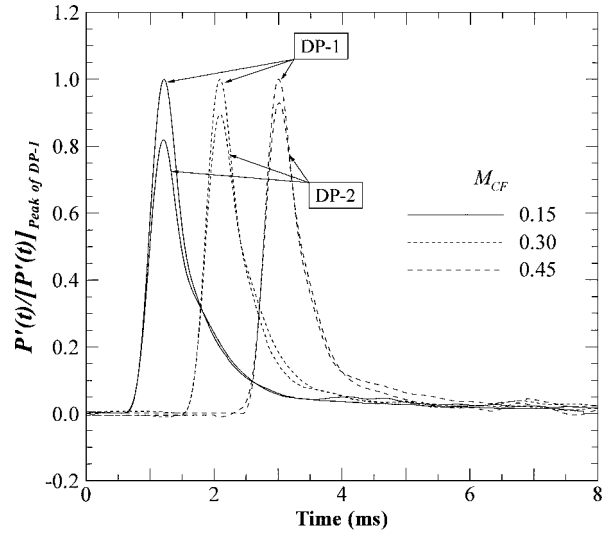

Fig. 13 Averages of DP-1 → DP-2 transmissions.

It is immediately apparent that the shapes of the DP-2 pulses are nearly identical to the incident DP-1 pulses, differing only by a slight peak amplitude reduction. In other words, the pulses pass through the engine with only a minor attenuation. This attenuation is diminished with increasing Mach number. Although these waves have no direct effect on the inlet flow, they are capable of producing additional reflections from later blade rows in multistage compressors and, thus, are of long-term interest.

Frequency Domain Analysis

The response of the engine to incident acoustic disturbances can be best characterized by the use of frequency-domain methods, specifically transfer functions. Given the time histories of the incident, reflected, and transmitted pressure disturbances, frequency-response functions (transfer functions) can be obtained as the ratio of the Fourier transforms of the output (reflected or transmitted) and input (incident) pressure histories:

$$H[f] = Z[f]/Y[f] = |H[f]|e^{i\phi[f]} \tag{4}$$

$H[f]$ and $\phi[f]$ are the amplitude gain and phase angle, respectively, of the complex transfer function representation.

This methodology is applicable if the relationship between the input and output functions is linear. This has been demonstrated to be the case for the small-amplitude acoustic disturbances considered here. The method takes advantage of all of the information contained in the experimental data. A single experimental run is sufficient to obtain response information as a continuous function of frequency. Importantly, the availability of a transfer function allows the prediction of the engine response to any arbitrary incoming acoustic disturbance. The method is highly developed, widely used in the acoustic characterization of duct components, and its details are available from numerous sources.[16] The codes required to calculate the transfer functions were readily available as part of the LabVIEW software package used in the data reduction.[18]

The (time-shifted and averaged) time histories of the pressure disturbances determined earlier served as inputs into the LabVIEW software. Because the code uses fast Fourier transforms (FFTs), the data sets were edited by adding trailing zeros to produce equally sized records with 2048 entries, corresponding to 16.4 ms of data.

Reflection

Figure 14 shows the amplitude gain of the average DP-1 → UP-2 reflection process for all Mach numbers tested. The data indicate an increasing reflection at all frequencies as the flow speed is increased, which was also evident from the time-domain data shown in Fig. 11. Depending on Mach number, the peak reflection occurs in the range 400–750 Hz, corresponding roughly to the inverse of the pulse duration.

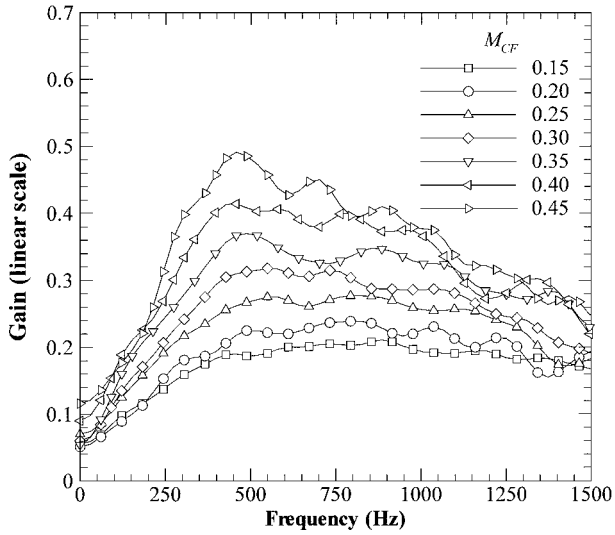

Fig. 14 Transfer function gain of DP-1 → UP-2 reflection.

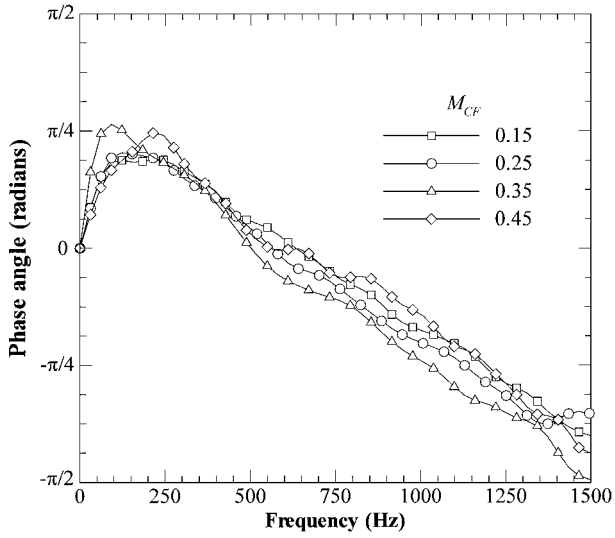

Fig. 15 Transfer function phase angle of DP-1 → UP-2 reflection.

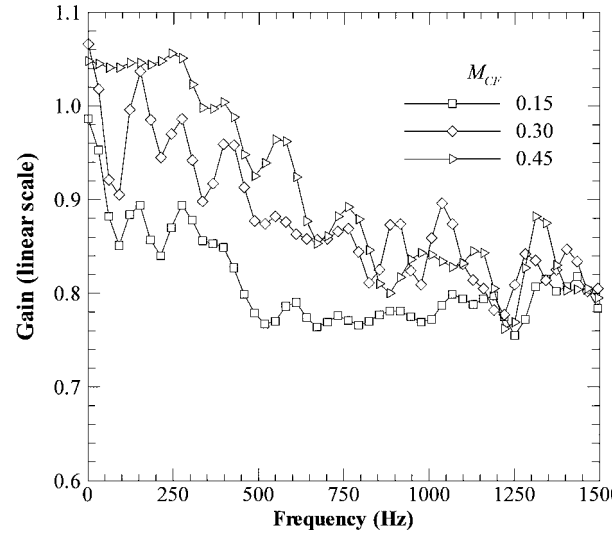

Fig. 16 Transfer function gain of DP-1 → DP-2 transmission.

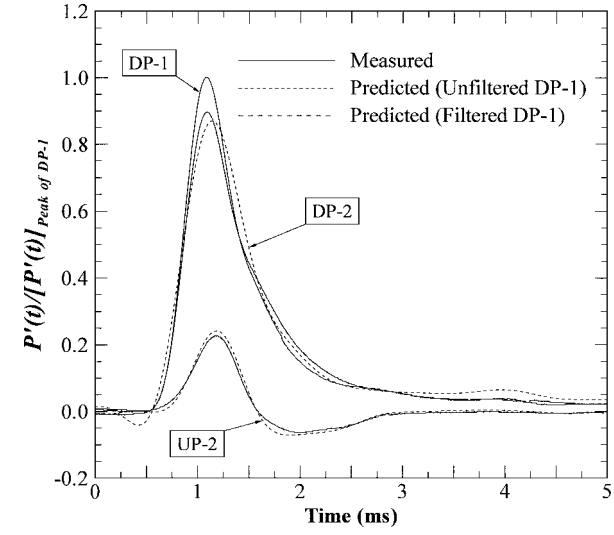

Fig. 17 Reconstruction of UP-2 and DP-2, $M_{CF} = 0.30$.

Figure 15 shows the phase angles of the transfer function as a function of frequency. This plot depends on the choice of the RRP location because the distance between the transducer and the RRP defines the overall time delay τ between the incident wave and the time-shifted reflection, as described by Eq. (3). In a frequency representation, the time delays affect the phase angle plot. This can be easily seen by considering that

$$\phi/2\pi = \tau/T \qquad \text{or} \qquad \phi = (2\pi\tau)f \tag{5}$$

Knowing the upstream/downstream propagation speeds, the information given is sufficient to construct a phase angle plot for any combination of the transducer/RRP locations.

Transmission

Figure 16 shows the gain of the transmission transfer functions, computed for the DP-1 → DP-2 transmission. The gains show a rising trend with Mach number and a declining trend with frequency. It is interesting that gains above unity were found at low frequencies.

The phase angles for the transmission are identically zero because we used the actual measured time delay to shift the transmitted wave back in time, forcing it to begin simultaneously with the incident wave. The formal evaluation of the phase angles confirmed this expectation, making an illustration unnecessary.

Prediction of Response to Arbitrary Incident Pulses

In possession of the transfer functions, it is possible to predict the response of the engine to arbitrary incident acoustic pulses, provided the pulse amplitude is in the linear range and its frequency content is within the bandwidth of the transfer function. Detailed explanations are left to any one of numerous available references[16]; the resulting reflection or transmission is given by a procedure symbolically defined by the following formula:

$$z(t) = \text{FFT}^{-1}\{H[f]^{*}\text{FFT}[y(t)]\} \tag{6}$$

A fully satisfactory demonstration of this capability would require another set of data, obtained with an incident pulse different from the one used to determine the transfer function. Such a demonstration has been successfully accomplished by Freund in a similar experiment.[12] Because of the inlet length and device positions chosen, no such alternate data set is readily available from the current effort. However, a limited demonstration is possible reconstructing the UP-2 and DP-2 pulses from DP-1, using the transfer functions illustrated in Figs. 14–16. If the method works, then the operations designated in Eq. (6) should reconstruct the measured data.

Figure 17 illustrates this reconstruction utilizing data recorded by the transducer at station 2 during a single run at $M_{CF} = 0.30$. In the first attempt, the unfiltered DP-1 pulse was used in Eq. (6). The main features of the responses are reproduced quite well, even though higher frequency contributions are seen to produce minor

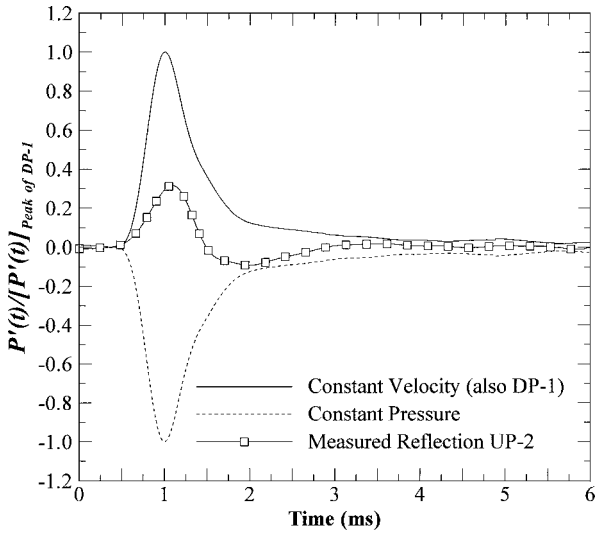

Fig. 18 Comparison of UP-2 with traditional boundary conditions at $M_{CF} = 0.45$.

deviations in the resultant pulse structures. In a second attempt, the filtered DP-1 pulse was utilized (which, as shown earlier, was nearly identical to the average pulse used to generate the transfer function in the first place). The resulting reconstruction is extremely accurate because it overlays both the measured UP-2 and DP-2 pulses to such a degree as to make them indistinguishable.

Figure 18 compares an experimentally determined reflected pulse with those predicted by the commonly employed constant pressure and velocity boundary conditions. The constant velocity condition produces a reflected pulse that is identical with the incident one, whereas the constant pressure condition produces a reflection that simply changes the sign of the incident pulse. These procedures correctly predict the duration of the reflected pulse (approximately the same as that of the incident one), but the magnitudes and shapes of the predictions are not even approximately correct. Clearly, neither of the two conventional boundary conditions provides a realistic simulation of the reflection process occurring at the compressor face.

Comments

The experimental data generated in this effort apply to a specific engine at various operating conditions and indicate that the response characteristics depend on the operating condition. Earlier experimental and analytical work has shown that the geometry of the engine is also an important variable. The transfer functions are, thus, engine specific, and each particular design project must use the transfer functions applicable to the engine intended for the system.

Because experimental determination is too costly for general use, methods will be required for the calculation of the required response characteristics (transfer functions). The development of such methods are still in their infancy; for example, the reflection coefficient given by the theory of Ref. 17 corresponds to the low-frequency limit of the transfer function, which should be adequate for slowly varying disturbances. Significant additional effort will be required to develop them to a mature level that allows their use in all practical flow situations.

Engine manufacturers are in the best position to develop the required methodologies because they are in possession of the required expertise and specific engine-related information. Providing boundary condition information to airframe manufacturers, along with the traditionally supplied operating parameters of the engine, would allow a significant improvement in the propulsion system design process. The data offered in the present paper represent appropriate benchmark information for testing such future methodologies and codes.

The transfer function method described in the present paper is capable of handling all frequencies that are likely to be of interest from an inlet dynamics point of view. However, it relies on a frequency-domain formulation, and its use requires an adaptation to the typical time-domain codes used in propulsion systems design. Analogous work has been published in the context of acoustic liners by Ozyoruk and Long[19] and by Tam and Auriault,[20] who developed methods for using frequency-domain information to formulate a wall boundary condition in a time-domain code. The present problem involves an outflow boundary condition. An appropriate extension of Ref. 19 is believed possible, but it represents a significant challenge and has not been attempted as part of this work.

Summary

The proper representation of a compressor as a boundary condition in an unsteady inlet code requires that the acoustic response of the compressor to incident acoustic disturbances be properly modeled. This requires the knowledge of the acoustic reflection coefficient of the compressor while in operation. The measurement of this quantity is best accomplished by the impulse method that requires the exploration of transients induced by the arrival of a short-duration acoustic disturbance (pulse) to the compressor face.

Detailed measurements were made of such transients using a single-stage axial flow compressor, for axial Mach numbers ranging from 0.15 to 0.45. The compressor was mated to a constant-area, circular inlet, in which the (compressive) pulses were initiated by the explosion of a thin wire. The incident acoustic pulse is highly axisymmetric, has a duration of 2 ms, and has a peak amplitude of approximately 3% of the mean static pressure measured at the compressor face. The pulse is free of variations of entropy and/or vorticity.

The measurements included the determination of both reflected and transmitted waves. The shape of the reflected pulse is similar to a single period of a strongly damped sine wave, with an amplitude much less than that of the incident pulse. The transmitted waves were found to be very similar to the incident pulses, showing only a minor attenuation in peak amplitude. The peak amplitudes of both the reflection and transmission were shown to increase with increasing Mach number, and the durations of both responses were found to be close to that of the incident disturbance.

Frequency-domain analysis was used to characterize the compressor face processes in terms of transfer functions, which offer a fairly complete description of the response characteristics. The principal factor affecting the transfer functions was the axial Mach number. No significant dependence was found on incident pulse strength, indicating that the system responds in a linear fashion. The transfer function representations permit the prediction of reflected and transmitted waves induced by arbitrary incident acoustic disturbances. A limited demonstration of this predictive capability was provided by reconstructing the reflected and transmitted waves from a given incident wave, using the experimentally obtained transfer functions.

An experimentally determined reflection was compared to predictions obtained using two currently customary CFBCs (constant pressure and constant velocity). The predictions are very poor, demonstrating that current practices intended to represent compressor face behavior during rapid transients need to be revised. The experimental data and processing methodology offered in this paper provide a sound basis for the development of more accurate CFBCs for incorporation into unsteady inlet codes.

Acknowledgments

This work has been sponsored by NASA Glenn Research Center under Grant NAG3-2087. Technical monitors for the program were, initially, Gary Cole and, later, John Slater, who saw the program to its conclusion. Additional financial support provided by The Boeing Company for facility modifications is gratefully acknowledged.

References

[1]Cole, G. L., "Atmospheric Effects on Inlets for Supersonic Cruise Aircraft," AIAA Paper 77-874, July 1977.

[2]Mayer, D. W., and Paynter, G. C., "Prediction of Supersonic Inlet Unstart Caused by Freestream Disturbances," *AIAA Journal*, Vol. 33, No. 2, 1995, pp. 266–276.

[3]Decher, R., Mayer, D. W., and Paynter, G. C., "Supersonic Inlet-Engine Stability," AIAA Paper 94-3371, June 1994.

[4]Cole, G. L., Melcher, K. J., Chicatelli, A. K., and Hartley, T. T., "Computational Methods for High-Speed Civil Transport: Inlet Controls/ Computational Fluid Dynamics Interdisciplinary Research," AIAA Paper 94-3209, June 1994.

[5]Clark, L. T., "Dynamic Response Characteristics of a Mixed Compression Supersonic Inlet as Part of a Larger System," AIAA Paper 95-0036, Jan. 1995.

[6]Mayer, D. W., and Paynter, G. C., "Boundary Conditions for Unsteady Supersonic Inlet Analyses," *AIAA Journal*, Vol. 32, No. 6, 1994, pp. 1200–1206.

[7]Sajben, M., and Freund, D. D., "Experimental Exploration of Compressor-Face Boundary Conditions for Unsteady Inlet Flow Computations," AIAA Paper 95-2886, July 1995.

[8]Freund, D., and Sajben, M., "Compressor-Face Boundary Condition Experiment: Generation of Acoustic Pulses in Annular Ducts," AIAA Paper 96-2657, July 1996.

[9]Freund, D., and Sajben, M., "Experimental Investigation of Outflow Boundary Conditions Used in Unsteady Inlet Flow Computations," AIAA Paper 97-0610, Jan. 1997.

[10]Sajben, M., and Freund, D. D., "Unsteady Inlet/Compressor Interaction Experiment to Support the Modeling of Compressor-Face Boundary Conditions," *Proceedings of the 8th International Symposium on Unsteady Aerodynamics and Aeroelasticity of Turbomachines*, Kluwer Academic, Norwell, MA, 1998, pp. 287–300.

[11]Freund, D., and Sajben, M., "Reflection of Large-Amplitude Acoustic Pulses from an Axial Flow Compressor," AIAA Paper 97-2879, July 1997.

[12]Freund, D. D., "Experimental Exploration of Compressor-Face Boundary Conditions for Unsteady Inlet Flow Computations," Ph.D. Dissertation, Dept. of Aerospace Engineering and Engineering Mechanics, Univ. of Cincinnati, Cincinnati, OH, Dec. 1997.

[13]Freund, D., and Sajben, M., "Experiment to Support the Formulation and Validation of Compressor-Face Boundary Conditions," *Journal of Propulsion and Power*, Vol. 16, No. 3, 2000, pp. 406–414.

[14]Kovasznay, L. S. G., "Turbulence in Supersonic Flow," *Journal of the Aeronautical Sciences*, Vol. 20, No. 10, 1953, pp. 657–675.

[15]Opalski, A. B., and Sajben, M., "High-Speed Inlet/Compressor System Response to Short-Duration Acoustic and Entropy Disturbances," AIAA Paper 2002-0372, Jan. 2002.

[16]Chung, J. Y., and Blaser, D. A., "Transfer Function Method of Measuring In-Duct Acoustic Properties. Part II, Experiment," *Journal of the Acoustical Society of America*, Vol. 68, No. 3, 1980, pp. 914–921.

[17]Sajben, M., and Said, H., "Acoustic-Wave/Blade-Row Interactions Establish Boundary Conditions for Unsteady Inlet Flows," *Journal of Propulsion and Power*, Vol. 17, No. 5, 2001, pp. 1090–1099.

[18]"Chapter 4: Measurement VIs," LabVIEW Analysis VI Reference Manual, National Instruments Corp., 1996, p. 19.

[19]Ozyoruk, Y., and Long, L., "Impedance Boundary Conditions for Time-Domain Computational Aeroacoustics Methods," AIAA Paper 97-0021, Jan. 1997.

[20]Tam, C. K. W., and Auriault, L., "Time-Domain Impedance Boundary Conditions for Computational Aeroacoustics," *AIAA Journal*, Vol. 34, No. 5, 1996, pp. 917–923.